Parametric gain in dispersion engineered photonic crystal waveguides

A. Willinger,[1,*] S. Roy,[2,3] M. Santagiustina,[2] S. Combrié,[4] A. De Rossi,[4] I. Cestier,[1] and G. Eisenstein[1]

[1]*Electrical Engineering Department, Technion Israel Institute of Technology, Technion City, Haifa, 32000, Israel*
[2]*CNIT, Dipartimento di Ingegneria dell'Informazione, Università di Padova, via Gradenigo 6b, Padova, 35131, Italy*
[3]*Department of Physics, National Institute of Technology, Warangal, 506004, India*
[4]*Thales Research and Technology, Route Départementale 128, 91767, Palaiseau, France*

[*]*amnon.willinger@gmail.com*

Abstract: We present a numerical simulation of parametric gain properties in GaInP PhC dispersion engineered waveguides in which the group velocity dispersion crosses zero twice and where the pump and the signal are $100ps$ pulses. The simulations use the M-SSFT algorithm which incorporates dispersive nonlinear coefficients and losses. We concentrate on narrow band parametric gain which occurs for pump wavelengths in the normal group velocity dispersion regime. The effects of structural details, of pump wavelength and of losses are carefully analyzed.

© 2013 Optical Society of America

OCIS codes: (050.5298) Photonic crystals; (060.4510) Optical communications; (190.4410) Nonlinear optics, parametric processes.

References

1. J. W. Li, T. P. O'Faolain, L. Gomez-Iglesias, A. Krauss, and T. F, "Systematic design of flat band slow light in photonic crystal waveguides," Opt. Express **16**, 6227–6232 (2008).
2. P. Colman, S. Combrié, G. Lehoucq, and A. De Rossi, "Control of dispersion in photonic crystal waveguides using group symmetry theory," Opt. Express **20**, 13108–13114 (2012).
3. N. A. R. Bhat and J. E. Sipe, "Optical pulse propagation in nonlinear photonic crystals," Phys. Rev. E **64**, 056604 (2001).
4. T. F. Krauss, "Slow light in photonic crystal waveguides," J. Phys. D: Appl. Phys. **40**, 2666 (2007).
5. T. Baba, "Slow light in photonic crystals," Nat. Photonics **2**, 465–473 (2008).
6. M. Santagiustina, C. G. Someda, G. Vadala, S. Combrié, and A. D. Rossi, "Theory of slow light enhanced four-wave mixing in photonic crystal waveguides," Opt. Express **18**, 21024–21029 (2010).
7. J. Li, L. O'Faolain, I. H. Rey, and T. F. Krauss, "Four-wave mixing in photonic crystal waveguides: slow light enhancement and limitations," Opt. Express **19**, 4458–4463 (2011).
8. I. Cestier, S. Combrié, S. Xavier, G. Lehoucq, A. D. Rossi, and G. Eisenstein, "Chip-scale parametric amplifier with 11db gain at 1550nm based on a slow-light gainp photonic crystal waveguide," Opt. Lett. **37**, 3996–3998 (2012).
9. B. Corcoran, C. Monat, M. Pelusi, C. Grillet, T. P. White, L. OFaolain, T. F. Krauss, B. J. Eggleton, and D. J. Moss, "Optical signal processing on a silicon chip at 640Gb/s using slow-light," Opt. Express **18**, 7770–7781 (2010).
10. I. Cestier, A. Willinger, V. Eckhouse, G. Eisenstein, S. Combrié, P. Colman, G. Lehoucq, and A. D. Rossi, "Time domain switching / demultiplexing using four wave mixing in gainp photonic crystal waveguides," Opt. Express **19**, 6093–6099 (2011).
11. C. Monat, B. Corcoran, C. Xiong, M. Collins, M. Pelusi, A. Clark, C. Grillet, J. Li, L. O'Faolain, T. Krauss, G. Marshall, M. Steel, D. Moss, and B. Eggleton, "Slow-light enhanced nonlinearities in photonic crystals and their application to optical signal processing and quantum integrated optics," in *Proceedings of the 17th Opto-Electronics and Communications Conference* (Busan, Korea, 2012) 885–886.

12. S. Roy, M. Santagiustina, P. Colman, S. Combrié, and A. De Rossi, "Modeling the dispersion of the nonlinearity in slow mode photonic crystal waveguides," Photonics J. **4**, 224–233 (2012).
13. I. H. Rey, Y. Lefevre, S. A. Schulz, N. Vermeulen, and T. F. Krauss, "Scaling of raman amplification in realistic slow-light photonic crystal waveguides," Phys. Rev. B **84**, 035306 (2011).
14. S. Roy, A. Willinger, S. Combrié, A. D. Rossi, G. Eisenstein, and M. Santagiustina, "Narrowband optical parametric gain in slow mode engineered GaInP photonic crystal waveguides," Opt. Lett. **37**, 2919–2921 (2012).
15. J. D. Harvey, R. Leonhardt, S. Coen, G. K. L. Wong, J. Knight, W. J. Wadsworth, and P. S. Russell, "Scalar modulation instability in the normal dispersion regime by use of a photonic crystal fiber," Opt. Lett. **28**, 2225–2227 (2003).
16. M. Marhic, K.-Y. Wong, and L. Kazovsky, "Wide-band tuning of the gain spectra of one-pump fiber optical parametric amplifiers," IEEE J. Sel. Top. Quantum Electron. **10**, 1133–1141 (2004).
17. D. Dahan and G. Eisenstein, "Tunable all optical delay via slow and fast light propagation in a raman assisted fiber optical parametric amplifier: a route to all optical buffering," Opt. Express **13**, 6234–6249 (2005).
18. A. S. Y. Hseih, G. K. L. Wong, S. G. Murdoch, S. Coen, F. Vanholsbeeck, R. Leonhardt, and J. D. Harvey, "Combined effect of kerr and raman nonlinearities on single-pump optical parametric amplifiers," in *Proceedings of the 33rd European Conference and Ehxibition of Optical Communication* (Berlin, Germany, 2007) 1–2.
19. E. Shumakher, A. Willinger, R. Blit, D. Dahan, and G. Eisenstein, "Large tunable delay with low distortion of 10 gbit/s data in a slow light system based on narrow band fiber parametric amplification," Opt. Express **14**, 8540–8545 (2006).
20. A. Willinger, E. Shumakher, and G. Eisenstein, "On the roles of polarization and raman-assisted phase matching in narrowband fiber parametric amplifiers," J. Lightwave Technol. **26**, 2260–2268 (2008).
21. E. Shumakher, A. Willinger, R. Blit, D. Dahan, and G. Eisenstein, "High resolution extraction of fiber propagation parameters for accurate modeling of slow light systems based on narrow band optical parametric amplification," in *Proceedings of Optical Fiber Communication Conference and Exposition* (Anaheim Convention Center, Anaheim, CA, USA, 2007).
22. G. K. L. Wong, S. G. Murdoch, R. Leonhardt, J. D. Harvey, and V. Marie, "High-conversion-efficiency widely-tunable all-fiber optical parametric oscillator," Opt. Express **15**, 2947–2952 (2007).
23. A. Gershikov, E. Shumakher, A. Willinger, and G. Eisenstein, "Fiber parametric oscillator for the 2 μm wavelength range based on narrowband optical parametric amplification," Opt. Lett. **35**, 3198–3200 (2010).
24. O. Sinkin, R. Holzlohner, J. Zweck, and C. Menyuk, "Optimization of the split-step fourier method in modeling optical-fiber communications systems," J. Lightwave Technol. **21**, 61–68 (2003).
25. A. Willinger and G. Eisenstein, "Split step fourier transform: A comparison between single and multiple envelope formalisms," J. Lightwave Technol. **30**, 2988–2994 (2012).
26. S. Mazoyer, J. P. Hugonin, and P. Lalanne, "Disorder-induced multiple scattering in photonic-crystal waveguides," Phys. Rev. Lett. **103**, 063903 (2009).
27. M. Patterson, S. Hughes, S. Combrié, N.-V.-Q. Tran, A. De Rossi, R. Gabet, and Y. Jaouën, "Disorder-induced coherent scattering in slow-light photonic crystal waveguides," Phys. Rev. Lett. **102**, 253903 (2009).
28. G. Agrawal, *Nonlinear Fiber Optics* (Academic Press, San Diego, 2001), Chap. 10, 389–444.

1. Introduction

The ability to engineer complex dispersion functions in photonic crystal (PhC) waveguides [1, 2] enables to enhance nonlinear processes by enacting slow mode operation [3–6]. Such enhancement is particularly large when the losses accompanying operation at large group index are small [2, 7] as has been recently demonstrated in a chip scale parametric amplifier which exhibits a gain of 11dB in a 1.5mm long GaInP PhC waveguide pumped with only 800mW [8]. Optical signal processing in integrated photonics circuits [9–11] has also been shown to be enhanced in specially designed nano-scaled waveguides.

The nonlinear response of complex dispersion engineered structures cannot be accurately modeled using simple schemes since both the nonlinear coefficients and the losses are highly dispersive. The effective nonlinear coefficient for self and cross phase modulation as well as four wave mixing (FWM) were calculated accurately in [12] where the dispersion of the Bloch modes and the tensorial nature of the nonlinear interactions were accounted for. The effect of loss dispersion was first considered in the context of Raman amplification in silicon PhC waveguides [13]. Extending the model in [12], Roy et al. [14] included wavelength dependent loss when modeling narrow band FWM (NB-FWM) in PhC waveguides with highly complex dispersion functions. NB-FWM is a very significant process that has been used extensively in

optical fibers [15–18] in the context of filtered amplification [16], slow and fast light propagation [17, 19, 20], fiber parameters characterization [21] and widely tunable parametric oscillators [22, 23].

   The model presented in [14] considered parametric processes under CW pump conditions. However, pulsed pumps are usually used in experiments and are naturally needed for switching and sampling applications [10]. Modeling nonlinear interactions with pulsed pumps requires spatially resolved simulation techniques, the most common being split step Fourier transform (SSFT). However, conventional SSFT [24] does not account for the dispersion of the nonlinear coefficient γ which in a complex waveguide may be very large. A new technique, termed M-SSFT [25] which uses multiple (coupled) envelopes propagating simultaneously, each comprising its own linear and nonlinear propagation parameters, is particularly suitable for calculating NB-FWM in complex dispersion engineered PhC waveguides. We have employed M-SSFT for calculating the parametric gain properties for a pulsed pump in a waveguide whose group velocity dispersion (GVD) crosses zero twice [2] and is therefore ideal for NB-FWM. The calculation includes wavelength dependent losses obtained from experiments and yields detailed gain properties for different dispersion functions.

2. Characteristics of dispersion engineered photonic crystal waveguides

The calculations we present in the following sections are performed for dispersion engineered, GaInP PhC waveguides described in [2,12]. A schematic diagram of the structure is presented in Fig. 1(a). It is based on a triangular lattice structure of air holes with a periodic spacing (lattice constant of the crystal) of $a = 465 nm$. The key parameter controlling the propagation properties is the position of the holes in the two innermost rows of the waveguide core which is set by an asymmetric shift T. This small perturbation couples an odd mode to the fundamental even mode, which is still confined in the waveguide, and thus modifies its propagation properties. The effects on the guided mode solutions can be calculated yielding the dispersion relation shown in Fig. 1(b) for five different values of the ratio T/a: 0.1, 0.125, 0.15, 0.175 and 0.2. The calculations assume a waveguide length of $1.3 mm$.

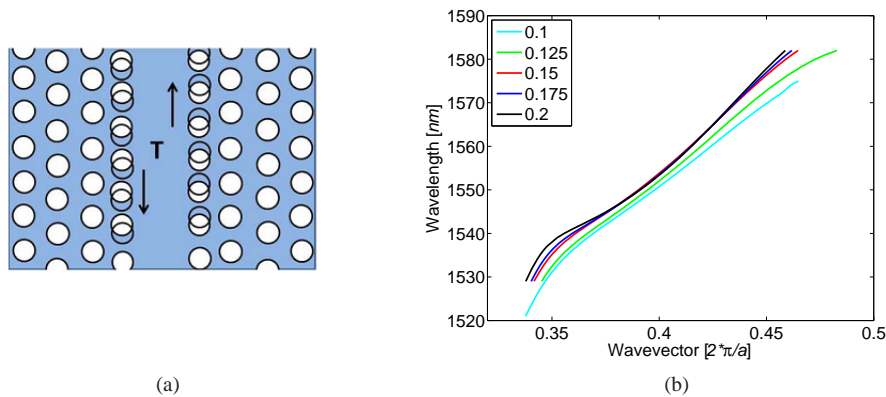(a)   (b)

Fig. 1. (a) Top view schematics of the PhC waveguide structure. The asymmetric shift T sets the position of the holes of two innermost rows. (b) Calculated band diagrams for the corresponding structures with the appropriate T/a values in the legend.

The spectral dependence of the group index n_g, the dispersion coefficient β_2, the loss coefficient α_{dB} (in units of $\frac{dB}{mm}$) and the nonlinear parameter γ_{SPM} for self-phase modulation (SPM) are presented in Fig. 2(a)-2(d), respectively. For each value of T, the group index of the guided modes was computed [12] for a set of wavelengths with $1nm$ spacing. The entire expression $\beta_1(\omega) = \frac{1}{c}n_g(\omega)$ was then approximated using a Taylor expansion around $\lambda_0 = 1545nm$ (Fig. 2(a)). The propagation constant $\beta(\omega)$ was expressed using a set of coefficients $\{\beta_m\}_{m=1}^M$, with M varying from 15 to 29. Large values of T yield complex n_g functions which require large values of M. The loss spectra (Fig. 2(c)) were based on measurements [14] after a fitting between losses and group index is performed; the short cut-off wavelength of the waveguide modes was set where $n_g = 5$ (in accordance with the light line of the PhC membrane). GaInP has a wide band gap (1.9eV) and therefore suffers from no two photon absorption. The observed losses at wavelengths where n_g is large are due to the modal change. Moreover, effects of backscattering related to structural disorder have a significantly larger impact at those wavelengths as has been investigated thoroughly in [26, 27].
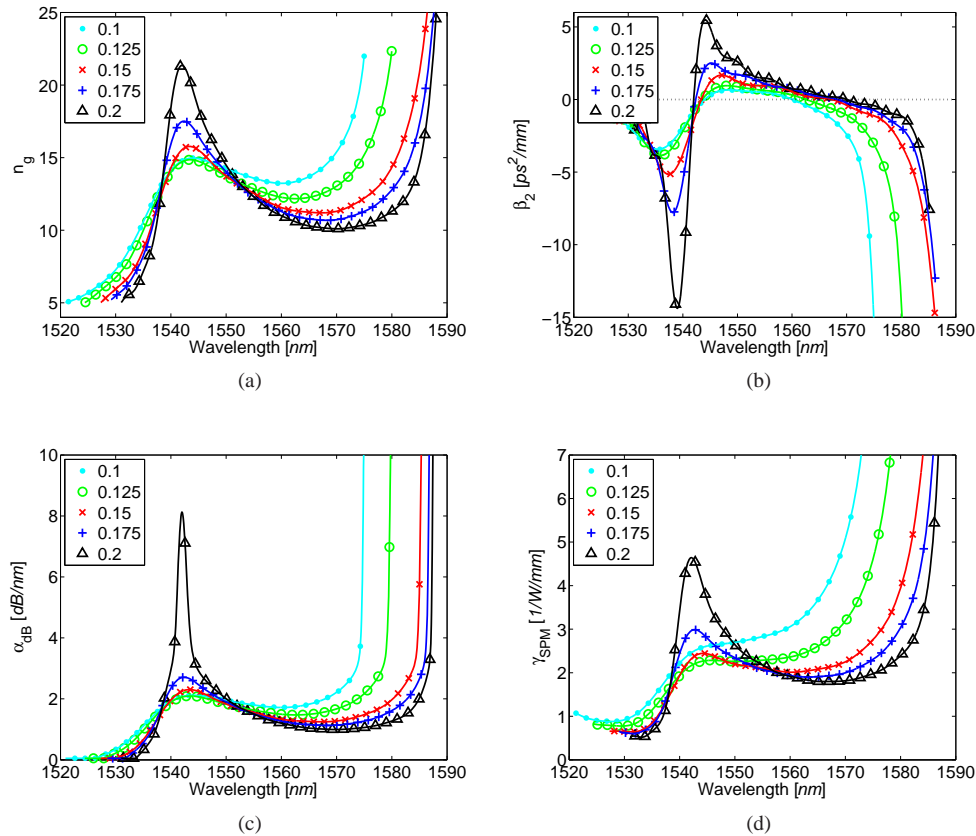

Fig. 2. Spectra of (a) Group index, (b) dispersion parameter, (c) losses and (d) SPM nonlinear parameter, all for different T/a values.

As detailed in [2, 12], the dispersion of the nonlinear properties is attributed to the variations in the mode distribution functions throughout the spectrum. Thus the waveguides are characterized by the modal dispersion of γ_{SPM} (Fig. 2(d)) and the other nonlinear parameters, which

were evaluated using the formalism of [12]. The dispersion of the nonlinear index can be neglected since the carrier wavelengths are far from the two photon absorption range of the GaInP medium, and so its value was fixed at $n_2 = 10^{-5} \frac{\mu m^2}{W}$.

From Fig. 2(b) we see that, for all waveguides, there is more than one zero-dispersion wavelength (ZDW). We define $\tilde{\lambda}_1$ and $\tilde{\lambda}_2$ (where $\tilde{\lambda}_1 < \tilde{\lambda}_2$) as the two ZDWs, and the wavelength region between them is that of normal dispersion ($\beta_2 > 0$), which is where the pump should be placed in order to generate NB-FWM [17]. By increasing the asymmetric shift T, the distance between the two ZDWs expands, and also, the group index n_g, the nonlinear parameter γ_{SPM} and the loss, all increase in a spectral region close to $\tilde{\lambda}_1$. Far from $\tilde{\lambda}_1$, however, these parameters decrease as T increases. A design with large T values is thus useful, for example, for all optical signal processing [9–11] where slow-light propagation and a large nonlinearity are desired. For NB-FWM, as we will show next, an enhanced nonlinearity throughout the spectrum is crucial to achieve larger gain.

3. Parametric gain mapping

We start by calculating the gain coefficient g for a set of pump and signal wavelengths using the FWM model [28] with CW pump, signal and idler waves (denoted hereon with subscript p, s and i respectively) and no losses. After incorporating dispersion of the nonlinear parameters, the square value of g is given by:

$$g^2 = (\gamma_F P_p)^2 - \left(\frac{\Delta \kappa}{2}\right)^2, \tag{1}$$

where P_p is the pump power and

$$\Delta \kappa = \Delta k + 2(\gamma_{ps} + \gamma_{pi} - \gamma_p) P_p \tag{2}$$

is the modified phase mismatch parameter which depends on the linear phase mismatch $\Delta k = \beta_s + \beta_i - 2\beta_p$ and on the nonlinear parameters originating from the various wave-mixing contributions (using the same notation as in the appendix of [12]): γ_p is the pump's SPM, γ_{ps} and γ_{pi} represent cross phase modulation (XPM) between the pump and the signal and idler respectively, and $\gamma_F^2 = \gamma_{sppi}\gamma_{ipps}$ represents the FWM term between all three waves.

Figure 3(a) shows qualitatively the behavior of $Re[g]$ for different pump and signal wavelengths, obtained with a pump power of $750mW$. The figure is basically a two dimensional map of the degree of phase matching conditions (when the expression in Eq. (1) is positive) for different T/a ratios. The phase matching conditions are calculated here assuming no losses. A more accurate calculation [14] considers the influence of losses on the phase matching. Since the losses of the waveguide at hand are small (with the exception of $T/a = 0.2$ where they exceed $4dB$ in a narrow spectral region), and since the calculation aims only at defining the spectral range where gain is available, Fig. 3(a) (based on Eq. (1)) suffices. The two waveguides with the largest T/a exhibit discontinuous phase matching maps since the signal and idler wavelengths needed to achieve phase matching fall outside the transmission band of the waveguide.

As stated before, larger values of T yield broader regions of normal dispersion, which is where the pump is set for NB-FWM. As the pump shifts away from both ZDWs, the parametric gain occurs in a narrow range of signal wavelengths (narrowband FWM) far from the pump wavelength. However, as the pump nears any one of the ZDWs, the phase matched signal wavelengths range widens (broadband FWM) and is closer to the pump wavelengths. This is better seen with the normalized maps in Fig. 3(b), which are plotted against the normalized detunings

$$\Delta_p = \frac{\lambda_p - \tilde{\lambda}_1}{\tilde{\lambda}_2 - \tilde{\lambda}_1}, \Delta_s = \frac{\lambda_s - \lambda_p}{\tilde{\lambda}_2 - \tilde{\lambda}_1}, \tag{3}$$
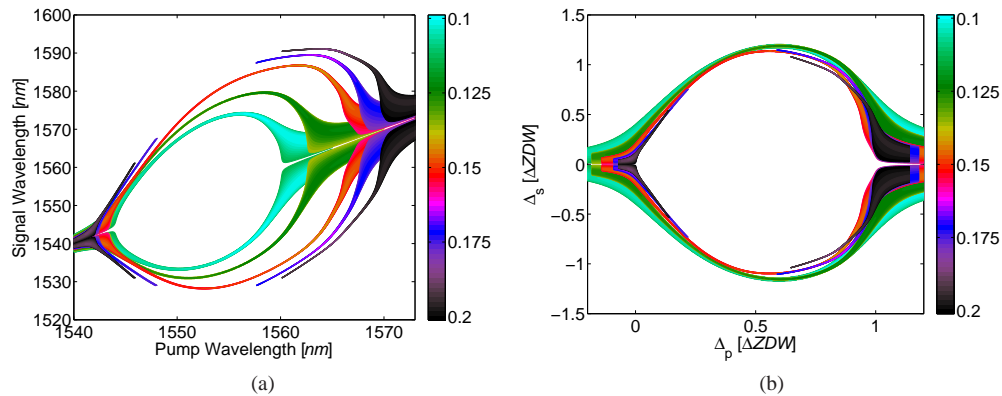
Fig. 3. Phase matching maps of the parametric gain coefficient with (a) absolute axis of the pump and signal wavelength and (b) normalized detunings (where $\Delta ZDW = \tilde{\lambda}_2 - \tilde{\lambda}_1$), for a pump power of $750mW$. The color scale indicates the different T/a values.

such that the axes are scaled to units of $\Delta ZDW = \tilde{\lambda}_2 - \tilde{\lambda}_1$.

The normalized maps suggest that for a given Δ_p, increasing T narrows the gain region. That said, we note that for all values of T/a, the normalized detuning Δ_s in which phase matching occurs is roughly the same. This can be attributed to the similar and scalable shapes of the group index curves (Fig. 2(a)) that determines the phase mismatch Δk. Though the real (quantitative) values of the parametric gain are not shown in Fig. 3(a) and 3(b), these phase matching maps will be used in section 4 since they offer a good assessment as to where one should position the pump wave in order to generate NB-FWM for a given signal wavelength.

4. Parametric amplification with pulsed pump and signal

The results of section 3 considered CW pumps and signals and lossless waveguides. Experimental characterization of nonlinear effects in PhC waveguides use always pulsed pumps and often also pulsed signals. Moreover, practical waveguides have losses which are dispersive. Calculation of the propagation characteristics of pump, signal and idler as well as of the parametric interaction under those conditions requires to use numerical computations. We use here the M-SSFT algorithm [25] which is advantageous over the conventional SSFT technique [24] which does not accommodate dispersive nonlinear coefficients. Moreover, since the waves are widely detuned from each other (as is typical of NB-FWM), M-SSFT reduces also the memory requirements and the computation time needed for the simulations. Dispersive losses are also incorporated into the model so that a complete description of the propagation is obtained.

We use $100ps$ wide pulses (extracted from a measured optical pulse) for both pump and signal with input peak powers of $750mW$ and $0.5mW$, respectively. For each waveguide with a specific T value, we sweep the pump wavelength between the two ZDWs and sweep the signal wavelength according to the negative and positive detuning boundaries of the phase matching map (depicted in Fig. 3(b)). Figure 4(a) shows the input (solid) and output (dash) pulse profiles of a signal (for one of many possible pump wavelength and signal detuning) in a waveguide with $T/a = 0.1$. We note that the signal experiences pulse compression which is caused by the time dependent pump. As long as the GVD between the two pulses is not too large, they overlap during most of their propagation in the waveguide. The peak of the signal pulse coincides with

the pump peak where the gain is large, while the leading and trailing edges experience a lower gain. This leads to the narrowing of the pulse profile.
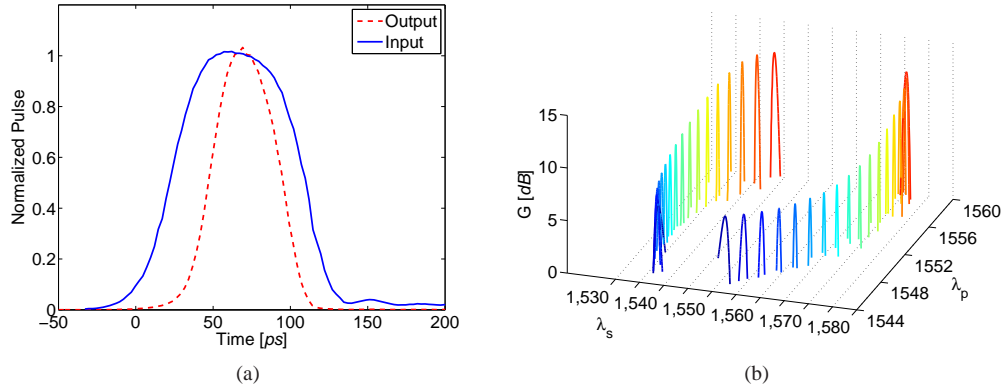

Fig. 4. Parametric gain of a pulsed signal with pulsed pump in a PhC waveguide with $T/a = 0.1$. (a) The input (solid) and output (dash) pulses belong to a signal at $\lambda_s = 1538.57nm$, with half-power width of $88.23ps$ and $45.74ps$ respectively. The pulsed pump is positioned at $\lambda_p = 1556.05nm$. (b) Gain spectra for different signal and pump wavelength.

Figure 4(b) shows gain spectra for several pump wavelengths in the same waveguide, and similar curves are obtained for other T/a ratios. In order to better characterize the different PhC waveguides we show, in Fig. 5(a) and 5(b) the parameters G_{peak} and λ_{peak} dependencies on pump wavelength. G_{peak} is the maximum obtainable gain value for a given pump wavelength; this gain is obtained for a signal wavelength λ_{peak}. The dependence of λ_{peak} on λ_p presents the same information as the phase matching maps in Fig. 3(a). Figures 5(a) and 5(b) can be combined into a map of the peak gain versus peak signal wavelength which is shown in Fig. 6(a). That figure represents the regimes of optimum amplification. Additionally, we show in Fig. 6(b) a map of the corresponding pulse width compression (defined as the ratio between the half-power width of the output pulse to that of the input) of the amplified signal at the gain peak wavelength.

As predicted in section 3, these engineered waveguides allow for NB-FWM for signals between $1528nm$ and $1586nm$. Though the phase matching maps in Fig. 3(a) show that phase matching exists for wavelengths longer than $1586nm$, the losses are large in this range and cannot be overcome by the gain. Matching the loss curves in Fig. 2(c), the peak gain for signal wavelengths longer than $1586nm$ is below $0dB$ in the waveguides with T/a of 0.15, 0.175 and 0.2. This also affects the peak gain of NB-FWM of short wavelengths (negative signal detunings) since the idler wave experiences those large losses. Hence, the losses cause narrowing of the wavelength range in which NB-FWM can be obtained.

As was noted in [14], the restricted normal dispersion regime in this waveguide limits the range of pump wavelengths since increasing the pump detuning from the short ZDW results in a reduced detuning from the second ZDW. Furthermore, for waveguides with large T values, the cut-off frequencies of the mode sets the boundaries of the signal detuning from the pump, and extreme losses for long wavelengths further diminish the gain. This is not the case for NB-FWM in optical fibers [17] where by increasing the detuning of the pump from the (single) ZDW, the signal detuning increases continuously to very large values.
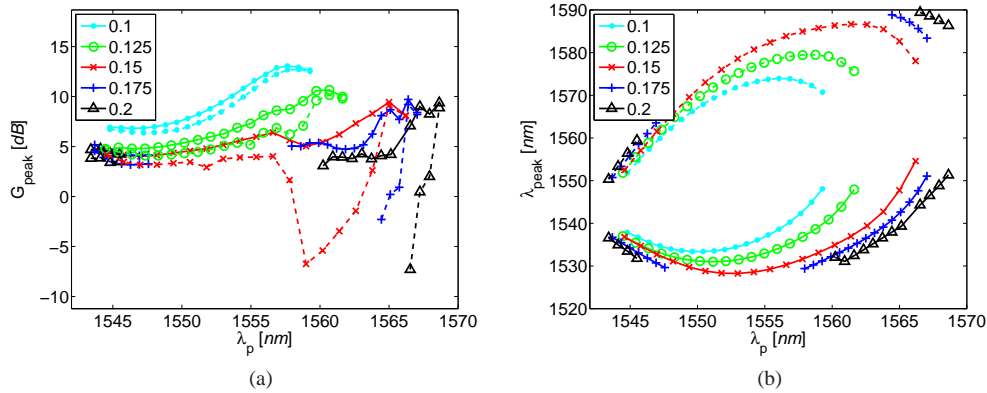
Fig. 5. Dependence on pump wavelength of (a) peak gain of NB-FWM and (b) the signal wavelength at which the peak gain is obtained. Different T/a values are shown, calculated in the presence of losses. Solid (dash) curves describe the peak gain and peak wavelength for negative (positive) detuning of the signal relative to the pump.
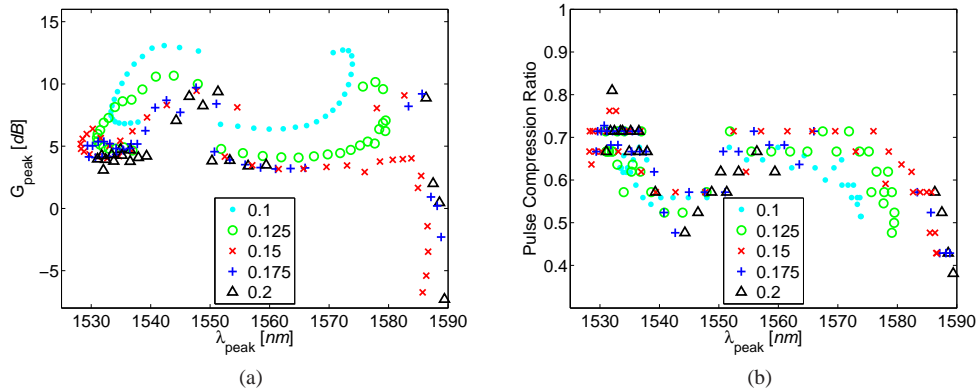

Fig. 6. Maps of (a) peak gain in NB-FWM versus peak signal wavelength and (b) pulse compression ratio versus peak signal wavelength in the presence of losses, for different T/a values.

The figures we presented suggest that choosing a waveguide with a large T/a ratio, from 0.1 to 0.15, results in a wide range of possible signal detunings due to the large normal dispersion region, yet with lower attainable gain. In order to evaluate the influence of T on the nonlinear coefficient and the gain, we use an analytical expression for the parametric gain in a lossless medium of length L, pumped at P_p

$$G = 1 + \frac{(\gamma_F P_p)^2}{g} sinh(gL).$$ (4)

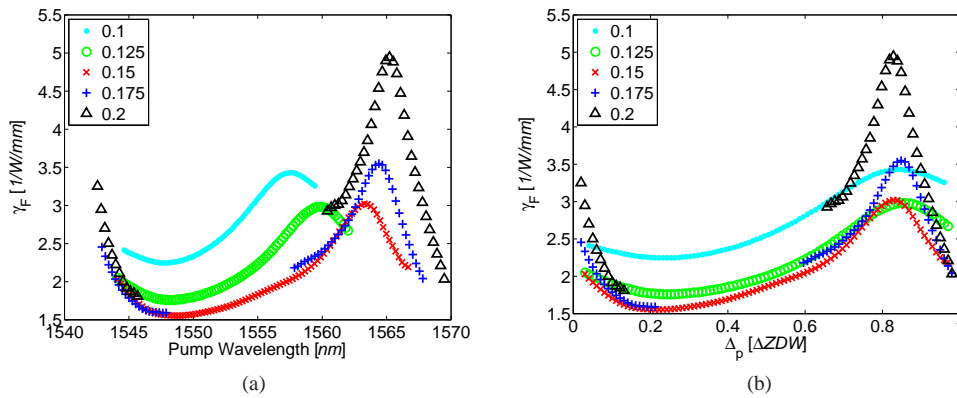The simple lossless case is sufficient here and yields the same conclusions as the comprehen-

Fig. 7. Spectra of the FWM nonlinear parameter γ_F as a function of pump wavelength (a) for an absolute wavelength scale and (b) for normalized detuning relative to the short ZDW (Δ_s). The different curves are given for different T/a values. The pump wavelength changes in the normal dispersion region and the signal wavelength is set to the mid-point detuning between the gain-region boundaries.
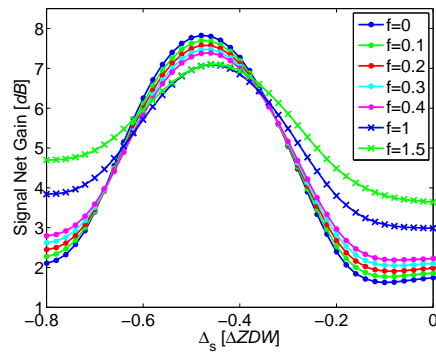

Fig. 8. Net gain spectra as a function of normalized signal-pump detuning Δ_s, for different loss values. The loss was increased by fixed factors f where the curve for $f = 0$ describes the lowest loss. $f = 0$ is actually the case of measured losses spectrum. The spectra are calculated for a pump wavelength $\lambda_p = 1546.37nm$ and $T/a = 0.1$. The net gain is the ratio between the output and input signal peak power divided by the linear loss factor.

sive analysis given in [14]. We show the values of γ_F as a function of the pump wavelength for an absolute wavelength scale (Fig. 7(a)) and also for a normalized detuning relative to the short ZDW (Fig. 7(b)). For each pump wavelength in the normal dispersion region, the signal is positioned in the middle of the gain region boundaries depicted in Fig. 3(a). As T increases, the values of these parameters reduce and thus the gain is lower. Though by increasing T we generate a slow-light region in the spectrum where n_g and γ_{SPM} are large, the nonlinear interactions between multiple wavelengths in the spectrum are weakened for large T values. As T increases

further, the nonlinear interactions for the pump wavelengths close to the long ZDW are also enhanced, yet the large losses suppress the signal gain. On the other hand, due to the stronger FWM interaction in waveguides with large T values, the pulse peak experiences a higher gain than its tails and so it is possible to achieve better pulse compression of the signal, down to 50% for positive gain (and down to 40% when the gain is less than unity).

A key issue in dispersion engineered PhC waveguides is maintaining low losses at wavelengths where the group index is large. The examplary family of waveguides analyzed here offers such properties. However, losses may increase due to design inaccuracies and various technological limitations. It is important therefore to examine the sensitivity of NB-FWM to propagation losses. To that end, we calculate the net gain (the output-to-input power ratio divided by the linear propagation losses) spectra for one case, $T/a = 0.1$, where the losses are increased by a fixed factor f (uniformly at all wavelengths) compared with those shown in Fig. 2(c). The results are shown in Fig. 8 for changing f between 10% to 150% (in the dB scale) such that $\tilde{\alpha}_{dB} = \alpha_{dB}(1+f)$. A loss increase reduces the net gain but the change is moderate and the system is found to be rather insensitive to reasonable changes in the loss. Thus the overall transmission of the signal is mainly impaired by linear losses.

5. Conclusion

To conclude, we have presented detailed numerical simulations of parametric amplification in a lossy dispersion engineered PhC waveguide with two ZDWs which are fed by pulsed pumps. The simulation uses the M-SSFT algorithm which is ideal for calculating NB-FWM in such complex waveguides since it allows for the incorporation of dispersive nonlinear propagation parameters as well as losses. Moreover, it improves significantly the computation efficiency for the widely detuned propagating signals typical of NB-FWM.

We explored the effect of changing the asymmetric shift parameter T in the waveguide design (presented in [12]) on the NB-FWM characteristics. We presented phase matching maps which describe the regions of broad and narrow band FWM, and showed that the normalized gain characteristics are relatively insensitive to the detuning between the two ZDWs (ΔZDW). By increasing T the maximum gain is reduced since the mixing efficiency between multiple modes with different wavelengths is reduced. The normal dispersion region between the two ZDWs widens as T increases which enables larger signal-pump detunings where gain is available, yet with very large T values the signal detunings pass the cut-off of the transmittance band. Increased losses at longer wavelengths further suppress gain and reduces the overall signal detunings span.

Pulse compression of the signal is observed in simulations due to the time-dependent pump envelope, and in waveguides with large asymmetric shift T, it is possible to reach pulse compression of up to 50%. Furthermore, the sensitivity of the NB-FWM system to changes in losses was examined. Though the losses may increase due to fabrication inaccuracies, the effect on the net gain proves to be small even for addition of 150% of the expected losses.